Liquid Crystals

DOI: 10.1002/anie.201209453

A Modulated Helical Nanofilament Phase**

*Ethan Tsai, Jacqueline M. Richardson, Eva Korblova, Michi Nakata, Dong Chen, Yongqiang Shen, Renfan Shao, Noel A. Clark, and David M. Walba**

The modern study of the liquid crystal (LC) phases formed by bent-core molecules[1] has led to many interesting and unexpected phenomena, including the first example of spontaneous reflection symmetry breaking and conglomerate formation in a bulk fluid phase.[2] Indeed, exploration of the unique behavior of bent-core materials is currently one of the most productive frontier research areas in soft matter science.[3] Perhaps the most complex of the known bent-core phases, the helical nanofilament (HNF) phase (also known as the B4 banana phase) has been under serious investigation since 1997,[1c,d] and continues to be a focus of interest in the bent-core materials constellation. Here, we report full characterization of the first example of a new phase in this family, $HNF_{(mod)}$, composed of simple alkoxybiphenylcarboxylate units and lacking the Schiff base groups found in previously known HNF mesogens.

The classic HNF phase possesses a unique hierarchical nanostructure: An assembly of twisted layers stacked to form well-defined chiral nanorods (individual HNFs ca. 40 nm diameter), with a structure driven by intra-layer frustration leading to spontaneous saddle splay, and formation of layers with negative curvature.[4–6] Solid state NMR data suggest that within individual HNF layers the structure is crystalline,[7] though electron diffraction shows that no interlayer positional correlation exists.[4] The HNFs in turn form a kind of hexatic LC phase, which freezes into a glassy state at ca. 110 °C. When the mesogens are achiral or racemic, an LC conglomerate of large heterochiral domains is easily seen in LC cells by polarized optical microscopy. The bulk HNF phase is porous,[4,6] and when grown in the presence of other materials, can produce nanostructured composites.[8] Potential applications of the HNF phase and composites include nonlinear optics, organic electronics, photovoltaics, and chiral separations.

Interestingly, of the great many bent-core structures reported to date, with the exception of a single reported outlier[9] all HNF mesogens include the hydrolytically unstable benzylideneaniline (Schiff base) moiety. This is problematic for some potential applications. Also, the rarity of the known HNF phases in the bent-core "structure space" motivates discovery of new HNF phases in order to better understand the molecular structural factors leading to their formation, and to allow future design of functional HNF materials.

Here we report characterization of seven homologues of biphenyl-3,4′-diyl bis-(4′-alkoxybiphenyl-4-carboxylate),[10] (diesters **1(*n*)** ($n = 9$–15), Figure 1a). All of these exhibit a new HNF phase possessing in-layer modulation in addition to the characteristic negative curvature of the layers.

Bent-core phases with in-layer modulation are known, including for example a tilted polar smectic (SmCP) phase possessing undulated smectic layers (also known as the B7 banana phase).[11] Here, we designate the new modulated HNF phase $HNF_{(mod)}$, with the proposed hierarchical structure for individual HNFs illustrated in Figure 1. As for the classic HNF phase, we propose that the aromatic cores in the new phase are tilted, while the tails are extended almost normal to the local layer plane.[4]

However, for the $HNF_{(mod)}$, in-layer modulation with a spacing of about 40 Å, not seen in the HNF phase, is suggested by experimental data. We propose this secondary modulation results from a structural periodicity with wave vector parallel to the layers and normal to the polar axis (**P**), as indicated in Figure 1c. The precise nature of this periodic defect structure is not known, though the lack of two-fold symmetry for rotation about ***b*** in diesters **1(*n*)** could reasonably produce such a periodic structural change by simple 180° rotation about ***b***, mediating in-layer "stripes" about eight molecules wide, as indicated (Figure 1c). Finally, as for the HNF phase, the twisted layers stack to form helical nanofilaments (Figure 1d).

Evidence for this structural picture of the $HNF_{(mod)}$ phase formed by diesters **1(*n*)** derives from: 1) polarized optical microscopy (POM); 2) differential scanning calorimetry (DSC); 3) X-ray diffraction (XRD) at small angle; and 4) transmission electron microscopy (TEM). The phase assignments, transition temperatures and enthalpies on cooling, and $HNF_{(mod)}$ layer spacing (d_1) and in-layer modulation dimensions (d_2) for diesters **1(*n*)**, are given in Table 1. A brief discussion of the key observations and interpretations leading to the model illustrated in Figure 1 follows.

As indicated in Table 1, all of the homologues are very similar in their basic behavior. All show a transition from isotropic to a more conventional bent-core phase, tentatively assigned as either a B1 (columnar) phase, or a B2 (tilted smectic) phase. For the lower homologues, ($n = 9$–12) the high temperature phases are monotropic with respect to $HNF_{(mod)}$.

[*] Dr. E. Tsai, Dr. J. M. Richardson, Dr. E. Korblova, Prof. Dr. D. M. Walba
Department of Chemistry and Biochemistry
University of Colorado, 215 UCB
Boulder, CO 80309-0215 (USA)
E-mail: walba@colorado.edu
Dr. M. Nakata, Dr. D. Chen, Y. Shen, R. Shao, Prof. Dr. N. A. Clark
Department of Physics, University of Colorado, 390 UCB
Boulder, CO 80309-0390 (USA)

[**] We thank the Liquid Crystal Materials Research Center (NSF MRSEC award no. DMR-0820579) for financial support of this work.

Supporting information for this article is available on the WWW under http://dx.doi.org/10.1002/anie.201209453.

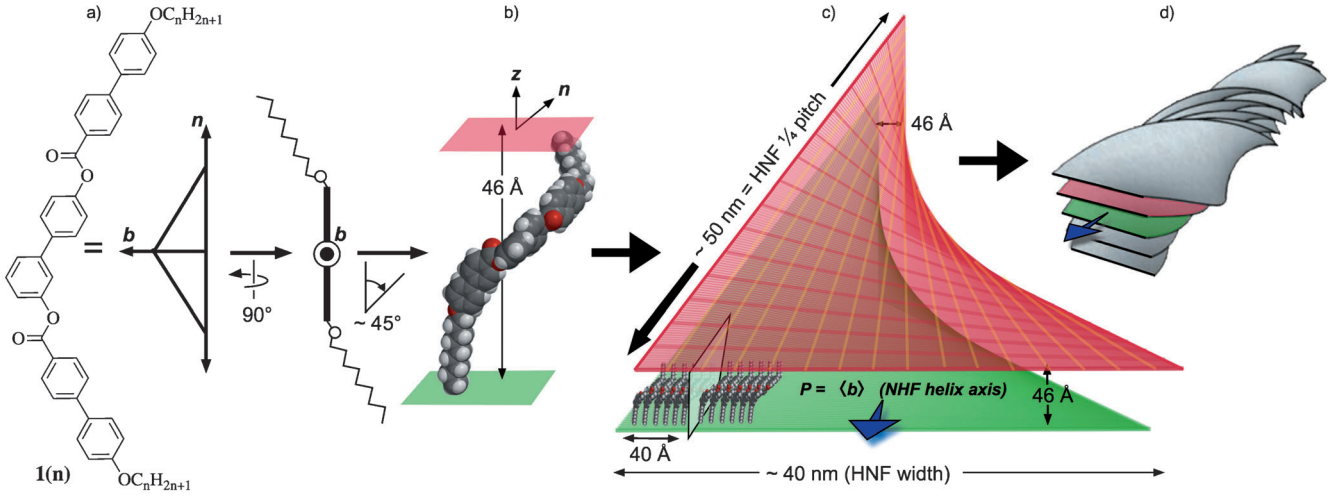

Figure 1. Hierarchical structure of the $HNF_{(mod)}$ phase, with metrics specific to diester **1(9)**. a) Chemical structure of diesters **1(*n*)**. b) Space-filling model of a reasonable conformation of **1(9)**, illustrating the proposed orientation of molecules in the smectic layers. c) Sketch of a single helical nanofilament layer bounded by doubly-ruled saddle surfaces (red and green) representing the HNF layer interfaces. Within the layer the molecules are organized into "stripes" which extend the entire length of the layer—indicated schematically by the blocks of tilted molecules at the bottom left of the graphic. d) Twisted layers stack to form HNFs. The layer width and the number of layers in a stack are limited by the free energy cost of less than ideal curvature, leading to nearly cylindrical HNFs.

Table 1: Phases, transition metrics, and HNF metrics for **1(*n*)**.

n	Phases, transition temperatures, and enthalpies[a]	d_1[b]	d_2[c]
9	$HNF_{(mod)}$–178→Iso (exotherm at 172) $HNF_{(mod)}$ (28.4)←166–B1 (18.5)←175–Iso	46.2	39.8
10	$HNF_{(mod)}$–172→Iso (exotherm at 164) $HNF_{(mod)}$ (27.4)←164–B1 (15.4)←167–Iso	48.3	41.9
11	$HNF_{(mod)}$–171→Iso (exotherm at 166) $HNF_{(mod)}$ (30.0)←164–B2 (19.6)←171–Iso	50.3	41.9
12	$HNF_{(mod)}$–174→Iso (exotherm at 166) $HNF_{(mod)}$ (29.2)←160–B1 (22.8)←172–Iso	52.8	41.9
13	$HNF_{(mod)}$–169→B1–172→Iso $HNF_{(mod)}$ (31.7)←160–B1 (20.8)←170–Iso	54.6	42.5
14	$HNF_{(mod)}$–167→B1–172→Iso $HNF_{(mod)}$ (33.6)←159–B1 (21.8)←170–Iso	55.6	41.9
15	$HNF_{(mod)}$–160→B1–168→Iso $HNF_{(mod)}$ (31.2)←151–B1 (20.4)←165–Iso	57.6	42.7

[a] Transition temperatures [°C] and enthalpies [kJ mol^{-1}] are taken from differential scanning calorimetry data.[12] [b] Layer spacing d_1 ($2\pi/q_1$, Å). [c] In-layer stripe spacing d_2 ($2\pi/q_2$, Å), measured from small-angle X-ray scattering (Figure 2d).

Elucidation of the detailed structure of these higher temperature phases has proven difficult, and is currently on-going. Strikingly, for the $HNF_{(mod)}$, while the layer spacing increases with increasing molecular length as expected, the in-layer modulation is essentially the same for all homologues.

The behavior of diester **1(9)** is illustrative (Figure 2).[12] On cooling from the isotropic phase a clear B1 texture can be seen by POM (Figure 2a). For this phase small-angle XRD (rotating anode) from "powder" samples in glass capillaries

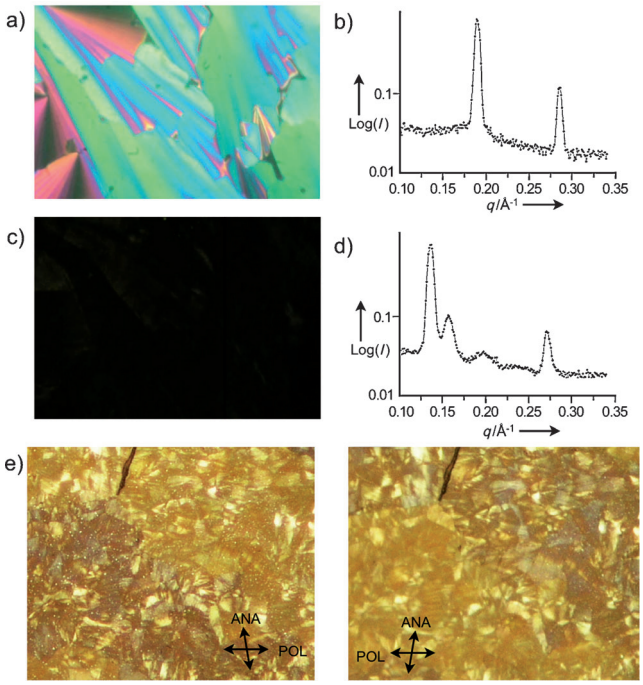

Figure 2. Data is for diester **1(9)**: a) Photomicrograph of the B1 texture seen by POM with crossed polarizer and analyzer (207°C, 4 μm glass cell, at 50× magnification). b) Log plot of the small-angle X-ray diffraction intensity (I) vs. scattering angle q for the B1 phase. c) Nearly optically isotropic texture observed for the $HNF_{(mod)}$ phase by POM at room temperature. d) Small-angle XRD log plot for the $HNF_{(mod)}$ phase showing three well-resolved peaks with sequentially lower scattering intensity with increasing q ($q_1 = 0.136$, $q_2 = 0.158$, and $q_3 = 0.198$ Å^{-1}). The very broad and weak fourth peak centered around $q = 0.24$ Å^{-1} is interpreted as resulting from a small amount of crystal phase, while the relatively large peak at $q = 0.273$ Å^{-1} is the second harmonic of q_1. e) Photomicrographs of the crystal phase of **1(9)** with analyzer and polarizer uncrossed, showing weak circular birefringence in heterochiral domains (room temperature).

shows two scattering vectors, supporting a tentative B1 phase assignment (Figure 2b). The major layer spacing indicated for this B1 phase is 33 Å ($q = 0.193$).

Further cooling into the $HNF_{(mod)}$ phase produces a texture almost perfectly isotropic in the plane (Figure 2c). The layer spacing of the this phase is 46.2 Å ($q_1 = 0.136$). Such layer expansion at the B1-HNF transition is fully consistent with the classic HNF behavior. However, for previously studied HNF phases only one peak is observed for the layers, while for all of the **1(*n*)** homologues the $HNF_{(mod)}$ phase exhibits three peaks (Figure 2d). The scattering vectors (q) of peaks 1, 2, and 3 (on increasing q) are related as $q_3 = \mathrm{SQRT}(q_1^2 + q_2^2)$, suggesting two different electron density waves in a rectangular lattice.

In the above XRD experiments the peak half width at half height (HWHH) for the major layer peaks is instrument resolution limited for both the B1 and $HNF_{(mod)}$ phases. However, high-resolution XRD experiments (Brookhaven synchrotron) run on powders of diester **1(14)** show an instrument resolution-limited HWHH in the B1 phase, consistent with the expected long-range layer ordering (correlation length = $\mathrm{HWHH}^{-1} \approx 600$ nm), and a much broader peak (correlation length ≈ 60 nm) for the $HNF_{(mod)}$ phase.[12] The relatively short-range order observed for the $HNF_{(mod)}$ layers is due to the limited diameter of the HNFs, and is consistent with high resolution XRD behavior shown by known HNF phases.

Interestingly, while the $HNF_{(mod)}$ phases of **1(*n*)** seem indefinitely stable once established, at least for some homologues a bulk crystalline conglomerate phase, difficult to obtain as a single pure phase, is nevertheless the thermodynamically most stable phase of the system (Figure 2e).[13]

The proposed $HNF_{(mod)}$ structure is confirmed by textural analysis of images obtained by transmission electron microscopy (TEM, Figure 3). For **1(9)**, cooling from an isotropic film on a glass substrate, followed by TEM imaging of the free surface by oblique evaporation of a thin film of metal, clearly shows the signature HNFs for the $HNF_{(mod)}$ phase (Figure 3a). Measurements taken from several individual HNFs in such images provide the HNF diameter and helix pitch given in Figure 1.[14]

The classic HNF phase of the double-benzylideneaniline NOBOW (P-9-O-PIMB: 1,3-phenylene bis[4-(4-nonyloxyphenyl-iminomethyl)benzoate),[1,2] shows a variety of interesting textures close to a glass surface, including flat lamellar textures, and "toric focal conics" possessing negative curvature, in addition to HNFs.[15] Imaging of the $HNF_{(mod)}$ phase of **1(10)** shows a lamellar texture close to the glass surface, but with clear topographical modulation normal to the layer plane (Figure 3b), with a periodicity 40 Å, providing strong support for the structure proposed in Figure 1.

Interestingly, in our hands it has proven impossible to grow long HNFs from neat samples of homologues of **1** other than **1(9)**. TEM investigation of **1(10)**, **1(12)**, and **1(15)** show a "broken HNF" texture, clearly exhibiting HNF fragments with negative layer curvature (Figure 3c), as is often seen for the NOBOW HNF phase. However, long HNFs were seen for **1(10)** and **1(15)** (the only homologues studied in this way) when the $HNF_{(mod)}$ phase was grown from 8-cyanobiphenyl

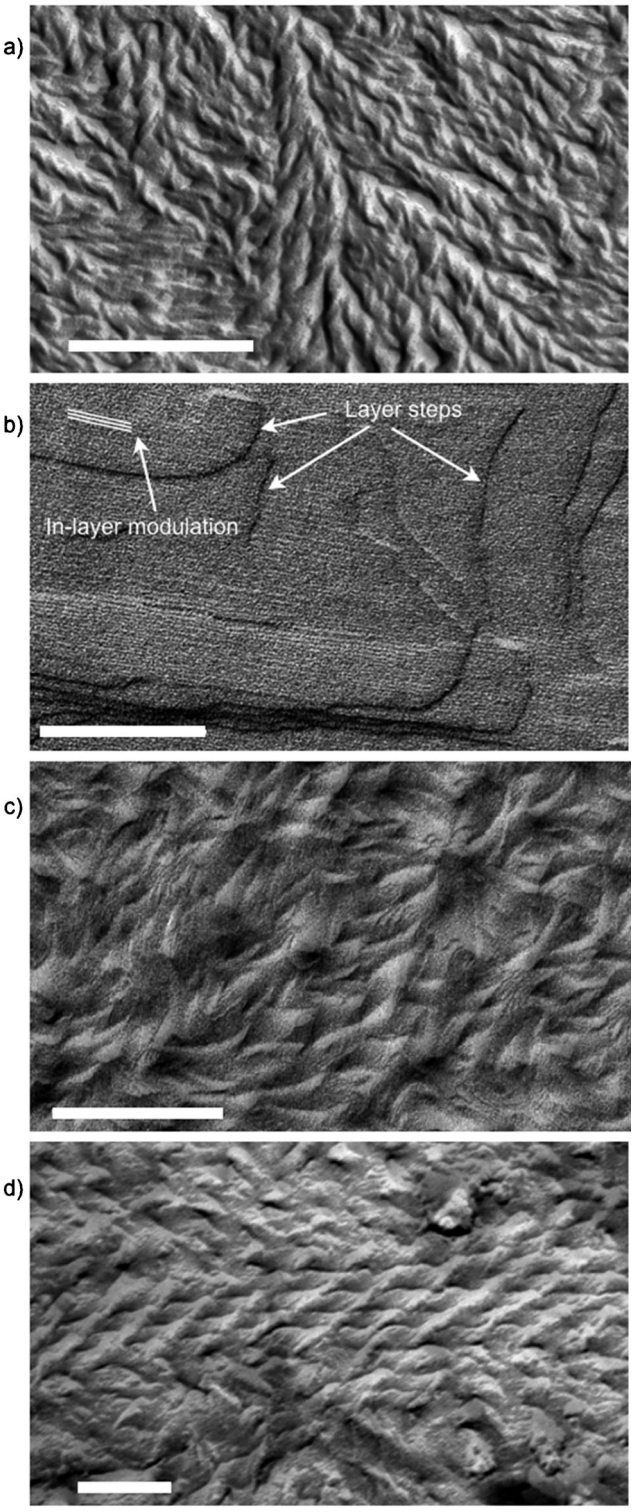

Figure 3. TEM images: a) Helical nanofilaments of **1(9)** grown at a free surface with air (scale bar 400 nm). b) Lamellar texture obtained from **1(10)** on a glass surface. The layers are parallel to the image plane, and the proposed in-layer stripes are clearly visible (scale bar 200 nm). c) Broken HNF texture obtained from neat **1(10)** (scale bar 200 nm). d) Helical nanofilaments obtained by growing the $HNF_{(mod)}$ phase from solution in 8-CB (75% 8CB by weight) (scale bar 100 nm).

(8CB) solution (Figure 3d). Growing the HNF phase of NOBOW from 8CB produces similar textures.[8d]

As mentioned above, a signature property of the classic HNF phase is formation of a conglomerate with large heterochiral domains easily seen by de-crossing polarizer and analyzer in POM experiments.[1b,c,4] Interestingly, these are not seen in neat $HNF_{(mod)}$ phases of diesters **1** by POM. The fact that the POM texture of **1(9)**, which forms very long HNFs (ca. 25 μm), is extremely dark with crossed polarizer and analyzer, suggests very little if any circular birefringence. This could be simply due to low rotatory power for this type of HNF. However, inability to observe large chiral domains by POM could be due to rapid nucleation of the phase relative to HNF growth, leading to uniformly chiral domains, which are small on the length scale of the wavelength of visible light. The latter interpretation gains support from the observation that $HNF_{(mod)}$ grown from solution does exhibit easily observable rotatory power in heterochiral domains.[16]

In conclusion, evidence for the formation of a new HNF phase, possessing in-layer modulation and lacking Schiff bases, formed by a homologous series of simple diesters is presented. This expands the demonstrated molecular "structure space" capable of providing the unique and potentially useful HNF phases—which represent a novel type of organic nanoparticle system. The $HNF_{(mod)}$ phase is very stable over a broad temperature range, though at least in some cases seems to be metastable with respect to a crystal phase. The geometry of the layer structure is similar to that of the classic HNF phase: Spontaneous negative curvature of the layers, limited in width to about 10 times their thickness. In addition, a structural supramolecular modulation normal to the helix axis is also present, as evidenced by XRD and TEM imaging data. The periodicity of the latter modulation is similar for all homologues, suggesting that this aspect of the $HNF_{(mod)}$ structure results from a similar packing of the cores. Additional studies designed to explore potential applications of the $HNF_{(mod)}$ phase of **1(*n*)**, and to extend the HNF mesogen structure space, which currently seems quite limited, are underway.

Received: November 26, 2012
Revised: January 26, 2013
Published online: April 19, 2013

Keywords: bent-core liquid crystals · ferroelectric liquid crystals · helical nanofilament phase

[1] a) T. Akutagawa, Y. Matsunaga, K. Yasuhara, *Liq. Cryst.* **1994**, *17*, 659; b) T. Niori, T. Sekine, J. Watanabe, T. Furukawa, H. Takezoe, *J. Mater. Chem.* **1996**, *6*, 1231; c) T. Sekine, T. Niori, M. Sone, J. Watanabe, S.-W. Choi, Y. Takanishi, H. Takezoe, *Jpn. J. Appl. Phys.* **1997**, *36*, 6455; d) T. Sekine, T. Niori, J. Watanabe, T. Furukawa, S. W. Choi, H. Takezoe, *J. Mater. Chem.* **1997**, *7*, 1307.

[2] a) D. R. Link, G. Natale, R. Shao, J. E. Maclennan, N. A. Clark, E. Korblova, D. M. Walba, *Science* **1997**, *278*, 1924; b) D. M. Walba, E. Körblova, R. Shao, J. E. Maclennan, D. R. Link, M. A. Glaser, N. A. Clark, *J. Phys. Org. Chem.* **2000**, *13*, 830; c) D. M. Walba, *Top. Stereochem. Mater. Chirality* **2003**, *24*, 457.

[3] a) G. Pelzl, S. Diele, W. Weissflog, *Adv. Mater.* **1999**, *11*, 707; b) L. Perez-Garcia, D. B. Amabilino, *Chem. Soc. Rev.* **2002**, *31*, 342; c) R. A. Reddy, C. Tschierske, *J. Mater. Chem.* **2006**, *16*, 907; d) H. Takezoe, Y. Takanishi, *Jpn. J. Appl. Phys. Part 1* **2006**, *45*, 597; e) J. W. Goodby, I. M. Saez, S. J. Cowling, V. Gortz, M. Draper, A. W. Hall, S. Sia, G. Cosquer, S.-E. Lee, E. P. Raynes, *Angew. Chem.* **2008**, *120*, 2794; *Angew. Chem. Int. Ed.* **2008**, *47*, 2754; f) J. Etxebarria, M. B. Ros, *J. Mater. Chem.* **2008**, *18*, 2919.

[4] L. E. Hough, H. T. Jung, D. Krüerke, M. S. Heberling, M. Nakata, C. D. Jones, D. Chen, D. R. Link, J. Zasadzinski, G. Heppke, J. P. Rabe, W. Stocker, E. Körblova, D. M. Walba, M. A. Glaser, N. A. Clark, *Science* **2009**, *325*, 456.

[5] a) D. B. Amabilino, *Science* **2009**, *325*, 402; b) I. Dierking, *Angew. Chem.* **2010**, *122*, 30; *Angew. Chem. Int. Ed.* **2010**, *49*, 29.

[6] E. A. Matsumoto, G. P. Alexander, R. D. Kamien, *Phys. Rev. Lett.* **2009**, *103*, 257804.

[7] D. M. Walba, L. Eshdat, E. Körblova, R. K. Shoemaker, *Cryst. Growth Des.* **2005**, *5*, 2091.

[8] a) Y. Takanishi, G. J. Shin, J. C. Jung, S. W. Choi, K. Ishikawa, J. Watanabe, H. Takezoe, P. Toledano, *J. Mater. Chem.* **2005**, *15*, 4020; b) N. A. Clark, et al., Presented at the 3rd Banana Workshop, Tokyo, Japan, **2007**; c) T. Otani, F. Araoka, K. Ishikawa, H. Takezoe, *J. Am. Chem. Soc.* **2009**, *131*, 12368; d) C. Zhu, D. Chen, Y. Shen, C. D. Jones, M. A. Glaser, J. E. Maclennan, N. A. Clark, *Phys. Rev. E* **2010**, *81*, 011704; e) D. Chen, C. Zhu, R. K. Shoemaker, E. Korblova, D. M. Walba, M. A. Glaser, J. E. Maclennan, N. A. Clark, *Langmuir* **2010**, *26*, 15541; f) D. Chen, J. E. Maclennan, R. Shao, D. K. Yoon, H. Wang, E. Korblova, D. M. Walba, M. A. Glaser, N. A. Clark, *J. Am. Chem. Soc.* **2011**, *133*, 12656; g) H. Nagayama, Y. Sasaki, F. Araoka, K. Ema, K. Ishikawa, H. Takezoe, *Soft Matter* **2011**, *7*, 8766; h) Y. Sasaki, Y. Setoguchi, H. Nagayama, H. Yao, H. Takezoe, K. Ema, *Physica E* **2011**, *43*, 779.

[9] E. Bialecka-Florjanczyk, I. Sledzinska, E. Gorecka, J. Przedmojski, *Liq. Cryst.* **2008**, *35*, 401.

[10] The 3,4′-biphenol core unit was first exploited by Tschierske et al. in the preparation of the first bent-core mesogens lacking the benzylideneaniline moiety: D. Shen, S. Diele, I. Wirt, C. Tschierske, *Chem. Commun.* **1998**, 2573. Synthesis of **1(*n*)** is described in the Supporting Information (Scheme SI-1 and detailed experimental).

[11] a) D. A. Coleman, J. Fernsler, N. Chattham, M. Nakata, Y. Takanishi, E. Korblova, D. R. Link, R. F. Shao, W. G. Jang, J. E. Maclennan, O. Mondainn-Monval, C. Boyer, W. Weissflog, G. Pelzl, L. C. Chien, J. Zasadzinski, J. Watanabe, D. M. Walba, H. Takezoe, N. A. Clark, *Science* **2003**, *301*, 1204; b) R. Amaranatha Reddy, M. W. Schroder, M. Bodyagin, H. Kresse, S. Diele, G. Pelzl, W. Weissflog, *Angew. Chem.* **2005**, *117*, 784; *Angew. Chem. Int. Ed.* **2005**, *44*, 774.

[12] POM data for **1(10)**–**1(15)** is presented in Section 2.2 (Figure SI-1) in the Supporting Information. DSC data for **1(9)**, **1(10)**, **1(13)**, and **1(14)** is presented in Section 2.3 (Figure SI-2) in the Supporting Information. XRD data for all **1(*n*)** is presented in Section 2.4 (Figure SI-3) in the Supporting Information.

[13] A brief discussion of the metastability of the HNF phase of compound **1(9)**, and the formation of the crystal phase illustrated in the photomicrographs in Figure 2e, is presented in Section 2.5 of the Supporting Information.

[14] Measurements of HNF thickness and half-pitch for **1(9)** and **1(15)** are given in Figure SI-4.

[15] D. Chen, M.-S. Heberling, M. Nakata, L. E. Hough, J. E. Maclennan, M. A. Glaser, E. Korblova, D. M. Walba, J. Watanabe, N. A. Clark, *ChemPhysChem* **2012**, *13*, 155.

[16] POM images of large conglomerate domains of **1(10)** grown from 8-cyanobiphenyl solution are given in section 2.6 (Figure SI-5) in the Supporting Information.

